Journal of Power Sources 196 (2011) 9884–9889

Contents lists available at ScienceDirect

Journal of Power Sources

journal homepage: www.elsevier.com/locate/jpowsour

Pt/C catalyst degradation in proton exchange membrane fuel cells due to high-frequency potential cycling induced by switching power converters

Masatoshi Uno*, Koji Tanaka

Institute of Space and Astronautical Science, Japan Aerospace Exploration Agency, Sagamihara, Kanagawa 252-5210, Japan

ARTICLE INFO

Article history:
Received 15 May 2011
Received in revised form 18 July 2011
Accepted 4 August 2011
Available online 11 August 2011

Keywords:
Electrochemical surface area (ECA)
Proton exchange membrane fuel cells (PEMFCs)
Potential cycling
Pt/C catalyst
Switching power converter

ABSTRACT

Proton exchange membrane fuel cells are operated using switching power converters that produce high-frequency ripple currents. These ripples cause high-frequency potential cycling of cells, which is believed to lead premature deterioration in the electrochemical surface area (ECA) of Pt/C catalysts. The qualitative relationship between ECA losses and the frequency of potential cycling was investigated in the range of 1 Hz to 1 kHz. For frequencies higher than 100 Hz, ECA losses were comparable with those at the potential hold condition. However, for lower frequencies, ECA decreased significantly with decreasing frequency. TEM observations showed that there was marked Pt particle growth for the 1-Hz cycling condition, whereas particle size distributions at 100 Hz and potential hold conditions were comparable. The currents associated with Pt oxidation and reduction during potential cycling were also investigated at various potentials and frequencies, and the charges associated with Pt loss (ΔQ) were determined by integrating the measured current. A correlation between the ECA trend and ΔQ was observed. The results obtained in this study are considered informative for electrical engineering research, because it relates to the design of switching power converters that do not negatively influence the Pt/C catalyst durability.

1. Introduction

Fuel cell voltages vary significantly with operating conditions, such as temperature, load current, stoichiometric ratio, and pressure. Therefore, switching power converters (i.e., dc–dc converters and dc–ac inverters) are generally used for converting the generated power of fuel cells and supplying power to the loads at a desired voltage level. Fig. 1 illustrates a schematic diagram of a fuel cell system using an inverter as a switching power converter. Switching power converters usually operate at high frequencies and generate corresponding high-frequency ripple currents (current fluctuations). The ripple frequency of inverters is generally found to be 100 Hz (120 Hz), which is the second-order harmonics of the utility frequency of 50 Hz (60 Hz) [1–3]. On the other hand, the ripple frequency of dc–dc converters is equal to the switching frequency of the converters, which is usually higher than several kilohertz. The ripple currents generated by the switching power converters are superimposed onto the fuel cell as shown in the inset of Fig. 1, and therefore, the fuel cell in the system operates at a certain dc current level with a superimposed ac ripple. The ripple current is regarded as a sort of load variations. Because fuel cell voltages significantly depend on the load current, the ripple current that is induced in the cell at high frequencies will result in variations in the voltage.

The effects of the high-frequency ripple currents generated by the switching power converters on the electrical characteristics of proton exchange membrane fuel cells (PEMFCs) and solid oxide fuel cells (SOFCs) have been investigated [4–9]. Previous studies based on simulation analyses reported that the interaction between the fuel cell and inverters deteriorates electrical characteristics, such as power factor, hydrogen utilization, and energy efficiency [4–7]. In addition, a negative impact of the high-frequency ripple on a membrane durability is also concerned [4]. A long-term experiment performed with an SOFC having a superimposed ripple current resulted in a premature increase in area-specific resistance [9].

A decrease in the electrochemical surface area (ECA) of Pt/C catalysts is widely known to be one of the major factors of PEMFC degradations [10–14]. Generally, the degradation of Pt/C catalysts is accelerated by potential variations that coincide with load variations and/or startup/shutdown sequences. Accelerated stress tests for ECA degradations have been performed extensively on the basis of potential cycling, which emulates load variations and/or startup/shutdown sequences, and the degradation mechanisms of Pt/C catalysts have also been studied in great detail [10–15]. Potential cycling tests are usually performed at a low-frequency range with a cycle period ranging from several seconds to several dozen seconds (i.e., <1 Hz). However, as mentioned above, in practical applications, not only the low-frequency potential cycling

* Corresponding author. Tel.: +81 50 3362 7510; fax: +81 42 759 8366.
E-mail address: uno.masatoshi@jaxa.jp (M. Uno).

0378-7753/$ – see front matter © 2011 Elsevier B.V. All rights reserved.
doi:10.1016/j.jpowsour.2011.08.030

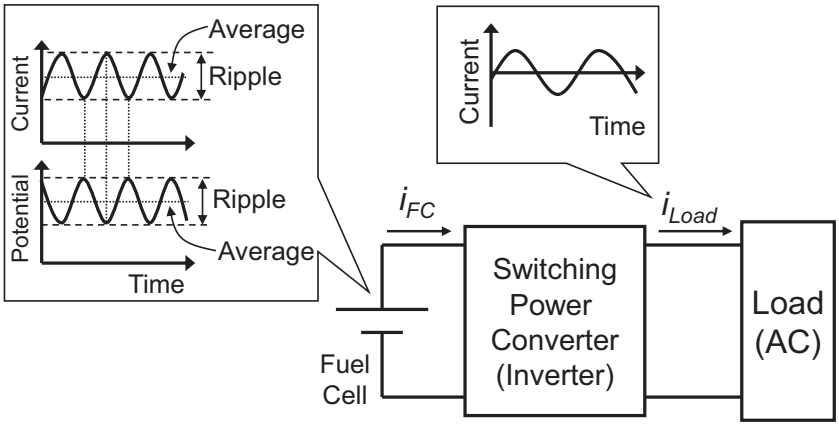

Fig. 1. Ripple current and cell potential variation for a fuel cell induced by an inverter in the fuel cell system.

due to load variations and/or startup/shutdowns but also the high-frequency potential cycling due to ripple currents generated by the switching power converters are induced onto the fuel cells. ECA degradation due to the high-frequency potential cycle is considered likely, but this issue has not been addressed so far.

The high-frequency ripple currents can be buffered using smoothing capacitors in the switching power converters. To mitigate the ripple current to negligible levels, capacitors with large capacitance are required [1,16]. However, larger capacitances result in huge, heavy, and expensive capacitors, which are not desirable. Several ripple mitigation techniques have been proposed and demonstrated for fuel cell systems [3,16–19]. However, they require advanced control techniques and additional circuit components, which imply increased system cost and design complexity. Thus, the correlation between ECA degradation and high-frequency potential cycling due to the ripple current should be considered for designing well-balanced fuel cell systems. From an electrical engineering viewpoint, determining proper switching frequency for switching converters is of primary importance, because the switching frequency significantly influences the converter performance in terms of power conversion efficiency, response characteristic, dynamic performance, noise emission, size, and weight.

The primary objective of this study is to investigate the qualitative relationship between Pt/C catalyst degradation and high-frequency potential cycling induced by switching power converters. The most unique parameter of the ripples is frequency, which is determined by the utility frequency and/or switching frequency. Therefore, this paper focuses on the ripple-frequency dependence of Pt/C catalyst degradations. The potential of the fuel cell was cycled for a frequency range of 1 Hz to 1 kHz, emulating the high-frequency ripples that are induced by switching power converters. The ECA degradation trend was obtained as a function of frequency. In addition, the current associated with Pt oxidation and reduction during potential cycling was also investigated at various potentials and frequencies, and the correlation between ECA degradation trends and the charge associated with Pt loss during cycling was discussed.

2. Experimental

The schematic diagram of the experimental setup for high-frequency potential cycling is illustrated in Fig. 2. The use of air as the cathode is realistic to emulate practical operating conditions. In potential cycling tests, the presence of oxygen in the cathode is found to have only minor effects on ECA loss [20]. To simplify the experiments, nitrogen was used instead of air. Humidified hydrogen and nitrogen with a relative humidity of 95% were supplied at a flow rate of 200 ml min^{-1} to the anode and cathode, respectively, of a fuel cell operated at 80 °C. For the experiments, we used a single cell having an active area of 25 cm^2 and single-serpentine flow channels each having a depth and width of 1.0 mm for both the anode and cathode flow fields. Membrane electrode assemblies (MEAs) consisted of Nafion 112 (DuPont), catalyst layers using 50 wt% Pt/C (Tanaka Kikinzoku Kogyo) with a Pt loading of 0.5 mg cm^{-2} on each electrode and 5 wt% Nafion ionomer (DuPont), and gas diffusion layers of 20 wt% polytetrafluoroethylene-proofed carbon paper (TGP-H-060, Toray). The cell potential was cycled using a combination of an in-house bipolar power source and function generator (FG-281, TEXIO). The potential waveforms during cycling were monitored using an oscilloscope (TDS2024, Tektoronix), and high-frequency potential cycling experiments were performed with an average potential, E_{ave}, and potential variation range, E_{var}.

E_{var} is one of the major factors that determine degradation in ECA. Generally, the surface of a Pt catalyst with a potential of approximately 0.4–0.6 V is bare and free from oxide species. However, at higher potential region, oxide growth takes place with a peak of 0.8 V and the oxide coverage increases with the potentials. Changes in the oxide coverage of Pt significantly affect the degradation rate, and transitions between the two regions can undermine Pt stability [11,21]. Previous studies revealed that the greater the range of potential variation, the greater will be the decrease in ECA [15].

In general, potential variations due to ripple currents that are generated by the switching power converters are smaller than those due to load variations or startup/shutdown sequences, although the magnitudes of the ripples depend on the design and application of the converters. In addition to the variation range, the average potential is dependent on load conditions. Technically, the potential variation range and average potential are determined by the ripple and average load current, respectively. To clarify the trend in degradation and the correlation between ripple frequency and degradation, this study adopted a potential cycling of 0.6–0.9 V, i.e., E_{ave} = 0.75 V and E_{var} = 0.3 V, which is the typical operating potential range of PEMFCs and is as large as that emulating load variations. Sinusoidal potential cycles were applied to a cell by a bipolar power source and function generator, as shown in Fig. 2. The high-frequency potential cycling tests were performed for a frequency range of 1 Hz to 1 kHz for 50 h. As a reference, we also performed a potential hold test with E_{ave} = 0.75 V. The CO_2 concentration in the cathode exhaust gas was monitored using a nondispersive infrared (NDIR) sensor (GMP 343, VAISALA) for observing the influence of high-frequency potential cycling on carbon corrosion, which also leads to decreases in ECA [11–14].

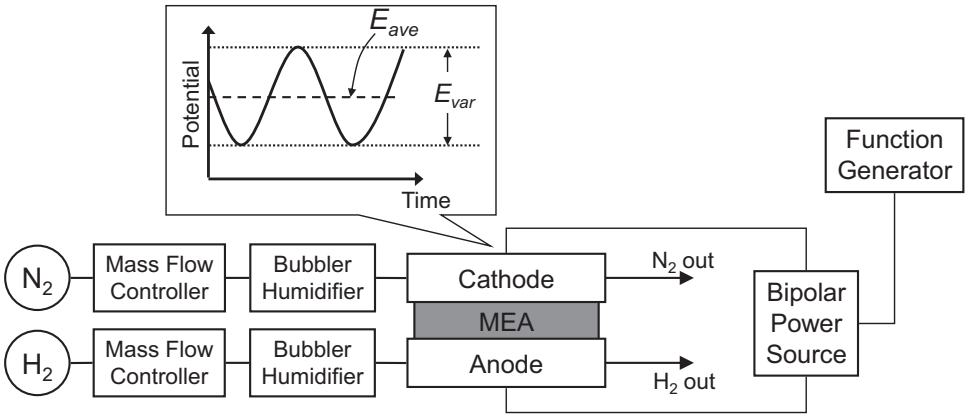

Fig. 2. Schematic diagram of the experimental setup and potential cycling profile for high-frequency potential cycling.

The retention factors of ECA of the cathode catalyst were periodically measured and determined by cyclic voltammetry (CV) using a potentiostat (1280C Electrochemical Measurement System, Solartron). The potential of the cell was swept at a scan rate of 50 mV s^{-1} between 0.06 and 0.9 V. The ECAs were calculated on the basis of the amount of measured charge that is associated with hydrogen desorption and with the assumption that the charge of a monolayer of adsorbed hydrogen on Pt is 210 μC cm^{-2} [22].

The cathode catalyst layers of pristine and aged MEA samples were examined and compared using transmission electron microscopy (TEM). TEM observations were performed in a HITACHI H-7100FA operated at 100 kV.

3. Experimental results

3.1. High-frequency potential cycling

Fig. 3(a) and (b) shows the trend of cyclic voltammograms for cells cycled at 1 Hz and 100 Hz, respectively. As the potential cycling tests progressed, the charge associated with hydrogen adsorption and desorption, which were observed for potential values lower than 0.4 V, gradually decreased. However, the charge associated with a double-layer capacitance (potential region around 0.4 V) did not change significantly. The charge for hydrogen adsorption and desorption decreased more significantly under the 1 Hz condition than under the 100 Hz condition, indicating that more significant degradation occurred at 1 Hz.

Fig. 4(a) and (b) shows ECA degradation trends as a function of time and frequency, respectively. The ECA retention ratios at the potential hold condition at each time instant are represented by dashed lines in Fig. 4(b). The ECAs consistently decreased as time elapsed. The ECA retention for lower frequencies decreased significantly, whereas those at frequencies higher than 100 Hz were almost identical to those at the potential hold condition. For example, the ECA at 1 Hz decreased to 73% after 50 h, while those at frequencies higher than 100 Hz and at the potential hold condition were approximately 91%. Although the number of cycles was very high at higher frequencies, the ECA losses were moderate when compared with those at low frequencies.

Generally, cycling the potential between the oxide formation and reduction region leads to degradation rates that are higher than those for potential hold conditions. Previous studies reported that the potential hold has minor effects on ECA losses and exhibits the lowest decay rate when compared with potential cycling

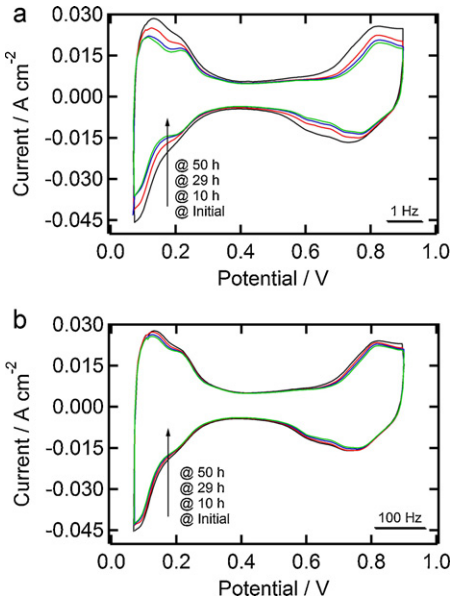

Fig. 3. Cyclic voltammograms for a cell cycled at (a) 1 Hz and (b) 100 Hz.

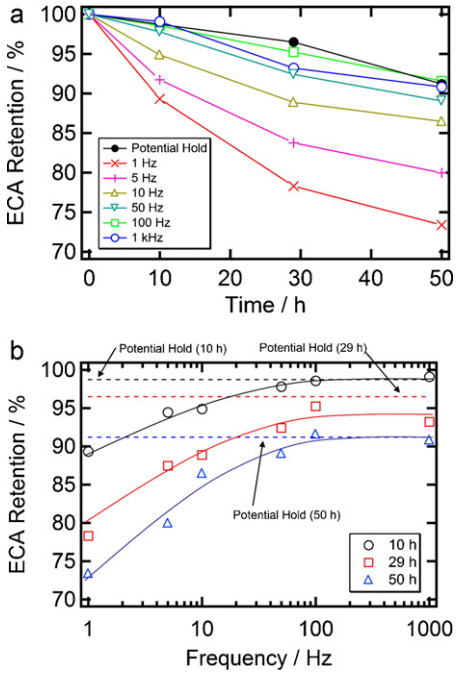

Fig. 4. Resultant ECA retention trends as a function of (a) time and (b) frequency.

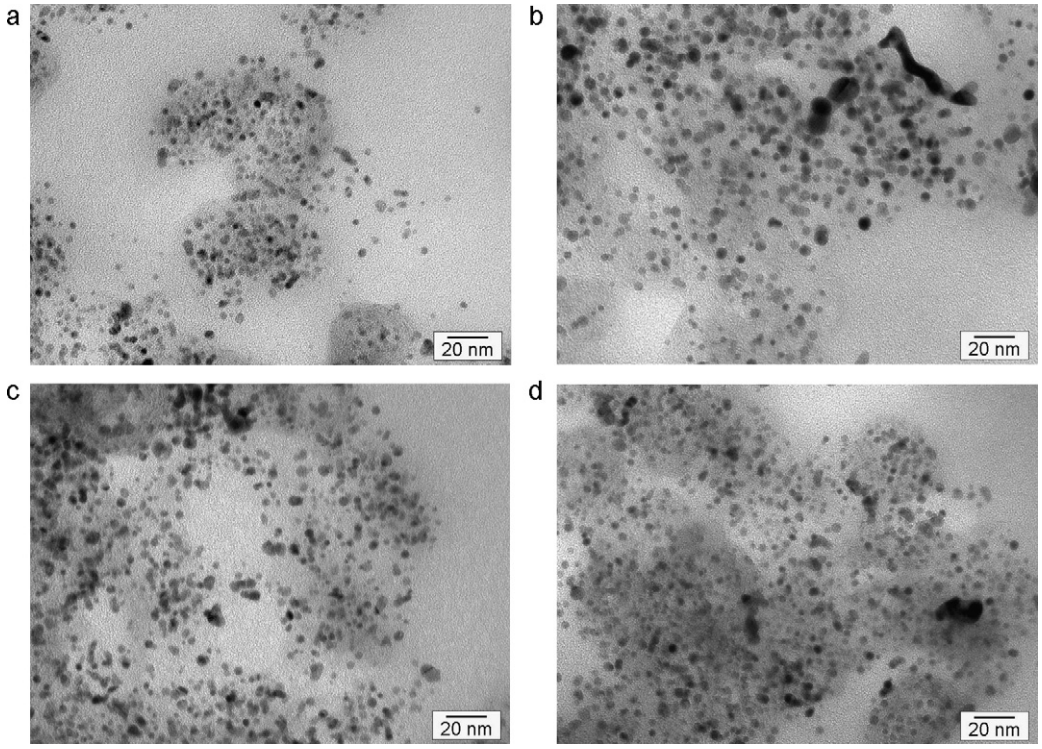

Fig. 5. TEM images of the cathode catalyst layer for (a) a pristine MEA, and MEAs after 50 h potential cycling at (b) 1 Hz and (c) 100 Hz, and (d) potential hold condition.

conditions [23]. For frequencies higher than 100 Hz, the ECA losses were comparable to those at the potential hold condition in spite of potential cycling. Hence, the potential cycles at high frequencies were not considered to be detrimental to Pt/C catalysts. However, for frequencies lower than 100 Hz, potential cycling resulted in accelerated ECA losses that were similar to those observed for conventional potential cycling, which emulates load variation and/or startup/shutdown cycles.

Fig. 5(a)–(d) shows representative TEM images from the cathode catalyst layer of MEAs before and after the high-frequency potential cycling tests. For the pristine MEA shown in Fig. 5(a), Pt nanoparticles (darker gray dots) that were homogeneously dispersed on carbon supports (brighter gray area) and having sizes of the order of 1–4 nm were observed. Subsequent to both cycling and potential hold conditions for 50 h, Pt particle sizes increased for all test conditions, and some agglomeration of individual Pt particles on the carbon supports was observed. The particle size for 100 Hz and potential hold conditions were comparable and ranged from approximately 1.5–4.5 nm, as shown in Fig. 5(c) and (d). The results imply that the potential cycle of 100 Hz did not have as negative an effect as the potential hold condition. However, for the 1 Hz condition, the particle size distribution was approximately 3–6 nm and there was marked particle growth, as shown in Fig. 5(b). This tendency was consistent with the trend in ECA loss shown in Fig. 4(b).

Fig. 6 shows the CO_2 concentration contained in the cathode exhaust gas during high-frequency potential cycling tests. The relatively large values detected at 0, 10, and 29 h were believed to be due to the temporary existence of air in the anode and/or cathode, because the experimental system was temporarily shutdown at those time instants. For all frequencies, concentrations of 7–8 ppm were detected, indicating that the carbon corrosion rate during the cycling tests was independent of cycle frequency. Therefore, carbon corrosion is not considered to be a factor influencing the frequency-dependent ECA loss trend shown in Fig. 4(b).

The result shown in Fig. 4(b) suggests that there is a proper frequency range at which the Pt/C catalyst is not negatively influenced by the potential cycle that is induced by the ripple current of switching power converters. For the cell and MEAs that were used for our experiments, the experimental results indicate that switching power converters should be designed to mitigate or even prevent ripple current generation at frequencies lower than 100 Hz. These results are expected to be of considerable interest to electrical engineers and researchers concerning the design of switching power converters for determining the converter's switching frequency and mitigating the ripple current components. However, because degradation trends are dependent on various operating parameters and MEA properties, an explanation of the frequency-dependent factor influencing the ECA degradation trends is necessary for application to power converter designs.

3.2. Frequency dependence of Pt oxidation and reduction

In general, electrochemical reactions take place at a specific time after potential variation. Darling et al. developed kinetic expressions for the Pt oxidation and dissolution reactions and demonstrated that the Pt oxide coverage does not rapidly attain equilibrium [24,25]. Uchimura et al. used asymmetric triangular

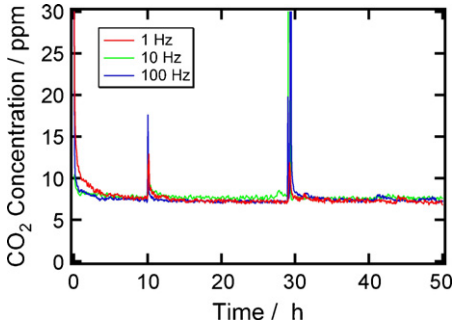

Fig. 6. CO_2 concentration in the cathode exhaust gas during potential cycling tests.

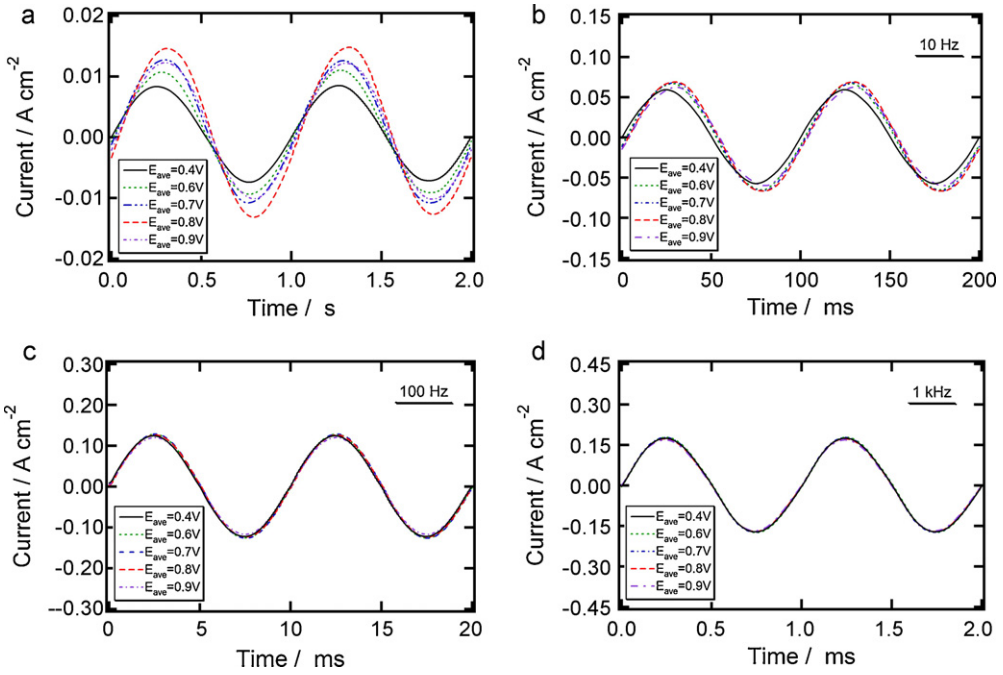

Fig. 7. Measured current waveforms during potential cycling with E_{ave} = 0.4, 0.6–0.9 V, and E_{var} = 0.05 V at (a) 1 Hz, (b) 10 Hz, (c) 100 Hz, and (d) 1 kHz.

waves for experimentally estimating the surface coverage of oxides on Pt film electrodes in 0.5 M sulfuric acid from measured currents during potential cycling, and they reported that the surface coverage does not change rapidly with time [21]. Imai et al. estimated the degree of oxidation of carbon-supported Pt nanoparticles in 0.5 M H_2SO_4 aqueous solution by integrating oxidation currents during a potential step [26], and the current associated with charging the double-layer capacitance was separated from the measured current for determining the oxidation current, and the Pt oxidation processes were estimated to take a long time after completing the double-layer charging process.

Based on the above-mentioned studies, we speculated that the Pt oxide coverage did not change by a great extent in the high-frequency range because of relatively short cycle periods, while the coverage at lower frequencies changed significantly because of longer cycle periods. In our study, to investigate the frequency and potential dependences of Pt oxidation and reduction currents, we measured the current responses of a cell using a pristine MEA during potential cycling with sinusoidal waves having E_{var} = 0.05 V and E_{ave} = 0.4, 0.6, 0.7, 0.8, and 0.9 V. These were measured using a current probe (TCP312, Tektronix) and data recorder (NR-HA08, KEYENCE) for a frequency range of 1 Hz to 1 kHz. Because the potential cycling with E_{ave} = 0.4 V and E_{var} = 0.05 V (i.e., 0.4 V ± 25 mV) is in the double-layer region, currents measured at E_{ave} = 0.4 V can be assumed to be the double-layer charging/discharging currents. Hence, the Pt oxidation and reduction currents can be estimated from the differences between measured currents at E_{ave} = 0.4 V and 0.6–0.9 V.

Fig. 7(a)–(d) shows the measured current responses at 1, 10, 100, and 1 kHz, respectively. At high frequencies (i.e., 100 Hz and 1 kHz), all measured current waveforms were almost identical and independent on the potential. At E_{ave} = 0.6–0.9 V, the measured currents are supposed to include currents associated with not only charging/discharging the double-layer capacitance but also Pt oxidation and reduction. Therefore, identical currents at all potentials indicate that the measured currents at 100 Hz and 1 kHz were dominated by the double-layer current. At lower frequencies, the magnitude of the measured current at E_{ave} = 0.6–0.9 V tended to be larger than that at E_{ave} = 0.4 V. In addition, the current responses at E_{ave} = 0.6–0.9 V lagged behind that at E_{ave} = 0.4 V. Assuming that the difference in the measured current between E_{ave} = 0.4 V and 0.6–0.9 V was used to either oxidize or reduce Pt, these results imply that Pt oxidation and reduction took place at low frequencies and lagged behind the charging/discharge of the double-layer capacitance.

Under potential cycling, the Pt is oxidized by water and dissolves during the reduction of Pt surface oxides, and the dissolution process during the anodic portion of the potential cycling is described based on the difference between anodic and cathodic charges in the surface oxidation and reduction of the Pt [27]. Mitsushima et al. performed potential cycling for a Pt wire in 1 M H_2SO_4 electrolyte in order to investigate the relationship between Pt consumption rates and the difference between the anodic and cathodic charges during potential cycling [27]. In their study, the Pt consumption rate was proportional to the difference between anodic and cathodic charges during cycling.

However, for potential cycling of MEAs, it is difficult to estimate the quantity of dissolved Pt in MEAs, because Pt is trapped in the membrane and/or ionomer in the catalyst layer [21]. Nevertheless, the difference between anodic and cathodic charges is considered to be a good index for estimating the Pt loss in the MEA during potential cycling. Measured currents during potential cycling, shown in Fig. 7(a)–(d), contain anodic and cathodic currents (or redox currents associated with Pt oxidation and reduction), i_{anodic} and $i_{cathodic}$, and hydrogen crossover current, i_{cross};

$$\begin{cases} i(t) = i_{anodic} + I_{cross} \quad (i_{anodic} > 0) \\ i(t) = i_{cathodic} + I_{cross} \quad (i_{cathodic} < 0) \end{cases} \tag{1}$$

where $i(t)$ is the measured current. I_{cross} was experimentally determined to be approximately 0.6–0.7 mA cm^{-2}. Anodic and cathodic charges per cycle, Q_{anodic} and $Q_{cathodic}$, can be expressed as

$$\begin{cases} Q_{anodic} = \displaystyle\int_0^{T_C} i_{anodic}\ dt \\ Q_{cathodic} = -\displaystyle\int_0^{T_C} i_{cathodic}\ dt \end{cases} \tag{2}$$

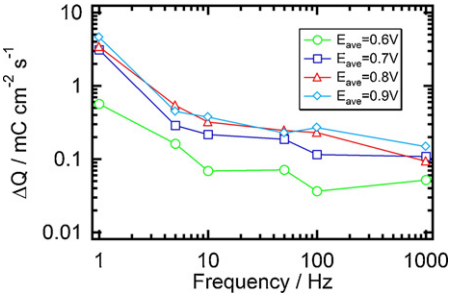

Fig. 8. Relationship between charges associated with Pt loss and frequency of the potential cycling.

where T_C is the cycle period. Because the high-frequency potential cycles in this study were performed at different frequencies, we have defined the difference between the anodic and cathodic charges per second, ΔQ, for the standardization from Eqs. (1) and (2) as

$$\Delta Q = \frac{Q_{anodic} - Q_{cathodic}}{T_C} = \frac{1}{T_C}\int_0^{T_C} \{i(t) - I_{Cross}\}\, dt \quad (3)$$

From the results shown in Fig. 7(a)–(d), ΔQ was determined using Eq. (3). Fig. 8 illustrates ΔQ as a function of cycle frequency. The lower the cycle frequency, the greater was the value obtained for ΔQ, implying that significant Pt losses occurred at low frequencies. ΔQ at E_{ave} = 0.6 V was the lowest for all frequencies, because 0.6 V is very close to the double-layer region, as can be seen in Fig. 3(a) and (b). At higher potentials (especially E_{ave} = 0.8 and 0.9 V), larger ΔQ values were observed, implying that Pt loss is likely at higher potentials. The resultant trend shown in Fig. 8 is in rough agreement with the results shown in Fig. 4(b); the larger the value of ΔQ, the greater the decrease in ECA. Although the experiment using MEAs is more realistic than that using liquid electrolytes, it is not suitable for quantitative investigations, as aforementioned. Therefore, similar studies using liquid electrolytes (which forms a part of our future research) should be performed for elucidating the quantitative frequency dependence of Pt loss during high-frequency potential cycling.

4. Conclusions

High-frequency potential cycling due to the high-frequency ripple currents that are generated by switching power converters is likely to be induced in PEMFCs. High-frequency potential cycling tests in the range 1 Hz to 1 kHz were performed for investigating the frequency dependence of ECA loss trends of cathode Pt/C catalysts.

The resultant ECA retention values at frequencies higher than 100 Hz were comparable with that at the potential hold condition. In contrast, ECA significantly decreased at lower frequencies, implying that there is a proper frequency range at which the Pt/C catalyst durability is not negatively influenced by potential cycling. The postmortem TEM observations showed that Pt nanoparticle size distributions at 100 Hz and at the potential hold condition were comparable, whereas marked growth in the size of the Pt particles was observed at 1 Hz.

We also investigated the currents associated with Pt oxidation and reduction during potential cycling at various potentials. The currents measured during potential cycling were integrated for determining the charge associated with Pt loss (ΔQ). An approximate correlation between the ECA loss trends and ΔQ was observed; the larger the value of ΔQ, the greater the reduction in ECA. Although the experiments using MEAs are more realistic than those using liquid electrolytes, further experiments using liquid electrolytes are necessary for investigating the quantitative relationship between Pt loss and the frequency of potential cycling.

The results obtained in this study are considered to be informative for electrical engineering and research aimed at determining a power converter's switching frequency, which is of primary importance in the field of electrical engineering. Proper determination of switching frequency would contribute to the mitigation of Pt/C catalyst degradation due to high-frequency potential cycling induced by ripple currents.

Acknowledgement

This work was supported by a Grant-in-Aid for Young Scientists (B) 21760723 from the Ministry of Education, Culture, Sports, Science and Technology (MEXT), Japan.

References

[1] M.E. Schenck, J.S. Lai, K. Stanton, IEEE Applied Power Electronics Conference and Exposition, 2005, pp. 114–120.
[2] S.R. Moon, J.S. Lai, S.Y. Par, C. Liu, IEEE Power Electronics Specialist Conference, 2006, pp. 1–6.
[3] C. Liu, J.S. Lai, IEEE Power Electronics Specialist Conference, 2005, pp. 2905–2911.
[4] G. Fontes, C. Turpin, S. Astier, T.A. Meynard, IEEE Trans. Power Electr. 170 (2007) 670–678.
[5] R.S. Gemmen, Trans. ASME 125 (2003) 576–585.
[6] W. Choi, G. Joung, P.N. Enjeti, J.W. Howze, J. Mater. Eng. Perform. 13 (2004) 257–264.
[7] W. Choi, J.W. Howze, P. Enjeti, J. Power Sources 158 (2006) 1324–1332.
[8] S.K. Pradhan, S.K. Mazumder, J. Hartvigsen, M. Hollist, Trans. ASME 4 (2007) 154–166.
[9] S.K. Mazumder, K. Acharya, C.L. Haynes, R. Williams, M.R. Spakovsky, D.J. Nelson, D.F. Rancruel, J.H. Hartvigsen, R.S. Gemmen, IEEE Trans. Power Electr. 19 (2004) 1263–1278.
[10] W. Schmittinger, A. Vahidi, J. Power Sources 180 (2008) 1–14.
[11] Y. Shao, G. Yin, Y. Gao, J. Power Sources 171 (2007) 558–566.
[12] J. Wu, X.Z. Yuan, J.J. Martin, H. Wang, J. Zhang, J. Shen, S. Wu, W. Merida, J. Power Sources 184 (2008) 104–119.
[13] S. Zhang, X.Z. Yuan, J.N.C. Hin, H. Wang, K.A. Friedrich, M. Schulze, J. Power Sources 194 (2009) 588–600.
[14] S. Zhang, X. Yuan, H. Wang, W. Merida, H. Zhu, J. Shen, S. Wu, J. Zhang, J. Hydrogen Energy 34 (2009) 388–404.
[15] R.L. Borup, J.R. Davey, F.H. Garzon, D.L. Wood, M.A. Inbody, J. Power Sources 163 (2006) 76–81.
[16] W. Shireen, R.A. Kulkarni, M. Arefeen, J. Power Sources 156 (2006) 448–454.
[17] Y. Wang, S. Choi, E. Lee, Electr. Power Energy Syst. 31 (2009) 43–49.
[18] S.K. Mazumder, R.K. Burra, K. Acharya, IEEE Trans. Power Electr. 22 (2007) 1437–1452.
[19] Y. Wang, S. Choi, E. Lee, J. Hydrogen Energy 34 (2009) 2340–2349.
[20] W. Bi, Q. Sun, Y. Deng, T.F. Fuller, J. Electrochem. Acta 54 (2009) 1826–1833.
[21] M. Uchimura, S. Sugawara, Y. Suzuki, J. Zhang, S.S. Kocha, ECS Trans. 16 (2008) 225–234.
[22] T.R. Ralph, G.A. Hards, J.E. Keating, J. Electrochem. Soc. 144 (1997) 3845–3857.
[23] C.H. Paik, G.S. Saloka, G.W. Graham, Electrochem. Solid-State Lett. 10 (2007) B39–B42.
[24] R.M. Darling, J.P. Meyers, J. Electrochem. Soc. 150 (2003) (1527) A1523–A1530.
[25] R.M. Darling, J.P. Meyers, J. Electrochem. Soc. 152 (2005) A242–A247.
[26] H. Imai, K. Izumi, M. Matsumoto, Y. Kubo, K. Kato, Y. Imai, J. Am. Chem. Soc. 131 (2009) 6293–6300.
[27] S. Mitsushima, S. Kawahara, K. Ota, N. Kamiyama, J. Electrochem. Soc. 154 (2007) B153–B158.